Laser consolidation: a rapid manufacturing process for making net-shape functional components

Xue, Lijue

Publisher's version / Version de l'éditeur:
https://doi.org/10.1533/9781845699819.6.492
Advances in Laser Materials Processing: Technology, Research and Application, pp. 492-534, 2010

Chapter 16: Laser Consolidation - A Rapid Manufacturing Process For Making Net-Shape Functional Components

Lijue Xue

Industrial Materials Institute, National Research Council of Canada

800 Collip Circle, London, Ontario, Canada N6G 4X8

Tel: (519) 430-7059; Fax: (519) 430-7064; E-mail: lijue.xue@nrc.gc.ca

16.1 Introduction

16.2 Process description

16.3 Microstructure and mechanical properties of laser-consolidated materials

16.3.1 Stainless and tool steels

16.3.2 Ni-based alloys

16.3.3 Ti-based alloy

16.3.4 Co-based alloy

16.3.5 Al-based alloy

16.4 Case studies of various industrial applications

16.4.1 Rotary cutting dies

16.4.2 Airfoils with embedded cooling channels

16.4.3 Net-shape functional sonar shells

16.4.4 Structural components for ARMS

16.4.5 Functional net-shape components for potential rocket engine applications

16.5 Future trend of the technology

16.6 References

16.1 Introduction

Free-form fabrication based on laser cladding process is an emerging computer-aided manufacturing technology that uses a laser beam to melt injected powder (or wire) to form a solid, functional component layer by layer. This one-step computer-aided manufacturing process does not require any moulds or dies, and therefore provides the flexibility to quickly change the design of the components. As a result, the lead-time to produce functional parts could be reduced significantly. As opposed to the conventional machining process, this new technology builds complete parts or features on a base component (or an existing component) by adding rather than removing material. The parts built using the technology are metallurgically sound, free of porosity or cracks. Various papers have been published by different institutions using laser cladding based free-form fabrication technology on several alloys and steels [1-7]. Although the technology has a great potential for many industrial applications, concerns about the surface finish and dimensional accuracy have been raised [8].

The Industrial Materials Institute of National Research Council of Canada (NRC-IMI) has developed a laser consolidation process that turns the laser cladding based free-form fabrication technology into a new elevation for enabling producing net-shape functional components that are difficult or even impossible to produce using conventional manufacturing technologies. Research work has been conducted on laser consolidation of various industrials materials (such as Ni-alloys, Co-alloy, Ti-alloy, Al-alloy, stainless steels and tool steels [9-15]) and its potential for various industrial applications [15-19]. In this chapter, an overview on NRC-IMI's work on laser consolidation research has been presented. The observation of unique microstructure along with functional properties of laser-consolidated materials has been discussed. In addition, some examples of laser consolidation process for making net-shape functional components for various potential industrial applications are presented.

16.2 Process description

The laser consolidation process requires a substrate (new base or existing component) onto which a part is built (Fig.1). A focused laser beam was irradiated onto the substrate to create a molten pool, while metallic powder simultaneously injected through a nozzle into the pool. A computer numerical control (CNC) motion system (3 to 5 axes) was used to control the relative movement between the laser beam and the substrate. The laser beam and the powder feed nozzle followed a pre-designed laser path based a computer aided design (CAD) model, creating a bead of molten material on the substrate, which solidified rapidly to form the first layer. The second layer was deposited on top of the first layer. By repeating this process, a solid thin wall structure was built up. When the laser path was designed properly to guide the laser beam movement, a complex shaped part can be built directly from a CAD model without any mould or die.

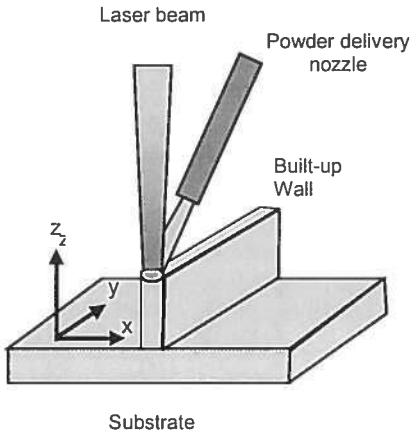

Fig. 1: An illustration of laser consolidation process.

A Lasag Nd:YAG laser coupled to a fiber-optic processing head was used for the laser consolidation work presented in this chapter. The laser was operated in a pulse mode with an average power ranging from 20 to 300 W. A Sultz-Metco 9MP powder feeder was used to simultaneously deliver metallic powder into the melt pool through a nozzle with the powder feed rate ranging from 1 to 30 g/min. All laser consolidation work was conducted at room temperature in a glove box, in which the oxygen content was maintained below 50 ppm during the process.

The microstructures of the laser-consolidated (LC) samples were examined metallurgically with an optical microscope as well as a Hitachi S-3500N Scanning Electron Microscope (SEM) equipped with an X-ray energy dispersive spectroscopy (EDS). A Philips X'Pert X-ray diffraction (XRD) system was used to identify the phases of the LC samples. A 100 kN Instron Mechanical Testing System was

used to evaluate the tensile and fatigue properties of the LC samples. Flat tensile and fatigue specimens were machined from LC thin wall coupons (about 0.8 - 1 mm in thickness). The specimen surfaces in the gauge length area were manually polished down to 600 grit. All tensile and fatigue tests were performed at room temperature as per respective ASTM standards. The microhardness of LC materials was measured with a Buehler Micromet II Microhardness Tester. A Falex ISC-200PC Pin-on-Disk System was employed to evaluate wear resistance of some LC materials as per ASTM Standard G99-95a. The amount of sample wear was determined by using a Dektak Surface Profiler to measure the cross-sectional depth profile of the wear scar. For each specimen, six to eight measurements were made in equal space along the whole wear scar and the average value of the wear loss area was then multiplied by the circumference of the wear scar to determine the wear volume loss of the sample. The amount of pin wear was determined by measuring the diameter of the circular wear scar on the ball to calculate the volume loss.

16.3 Microstructure and mechanical properties of laser-consolidated (LC) materials

16.3.1 Stainless and tool steels

Stainless steel – 316L

Low carbon austenite 316L stainless steel (S.S.) is widely used for various corrosion resistant applications. The 316L S.S. powder used for laser consolidation contains 0.024% C, 16.4% Cr, 10.4% Ni, 2.23% Mo, 1.42% Mn and 0.45% Si. The LC 316L S.S. consisted of fine cellular dendritic microstructure resulting from the rapid solidification inherent to the laser consolidation process (Fig.2). The cellular grain growth occurred in random orientations. The XRD analysis showed that the LC 316L S.S. had exactly the same γ phase as the powder used: face-centered cubic structure with a lattice parameter of about 3.59Å (Fig.3). In addition, both XRD results and optical microscopic observation revealed no preferred orientation observed in the LC 316L S.S.

The tensile properties of LC 316L S.S. along horizontal and vertical directions were almost the same due to no preferred microstructure orientation (Table 1). Along the horizontal and vertical directions,

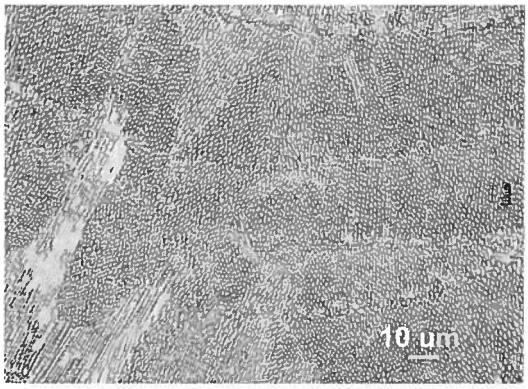

Fig.2: Optical microstructure of LC 316L stainless steel.

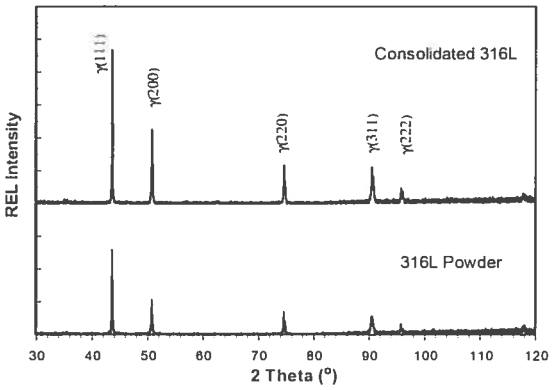

Fig.3: Comparison of XRD pattern of LC 316L stainless steel with powder form.

the average yield strength of LC 316L S.S. was 344 MPa and 328 MPa, while tensile strength was 560 MPa and 540 MPa, respectively. The elongation of the LC sample was 35% along the horizontal direction and 43% along the vertical direction. The LC 316L S.S. demonstrated higher yield strength as compared to the cast or the wrought material [20-21], while the tensile strength and elongation were comparable.

8Table 1: Tensile properties of LC 316L stainless steel

Conditions		$\sigma_{0.2}$ (MPa)	σ_{UTS} (MPa)	δ (%)
As-consolidated 316L	Horizontal	344	560.	35
	Vertical	328	540	43
Cast 316L (CF-3M) [20]		262	552	55
Hot finished & annealed 316L bar [21]		170	480	40
Cold finished & annealed 316L bar [21]		310	620	30

Tool steel - H13

H13 is a hot work tool steel that has good resistance to thermal fatigue, erosion and wear, and is widely used for making molds and dies. The H13 powder used for laser consolidation contains 0.42% C, 5.04% Cr, 1.33% Mo, 1.06% V and 0.88% Si. LC H13 samples were metallurgically sound and free of cracks or porosity. LC H13 tool steel showed directionally solidified dendritic microstructure with layered features: very fine columnar dendrites (around 1–2 µm in dendritic arm spacing) aligned along vertical direction (Fig.4a). Cellular features were observed along the transverse cross-section (Fig.4b).

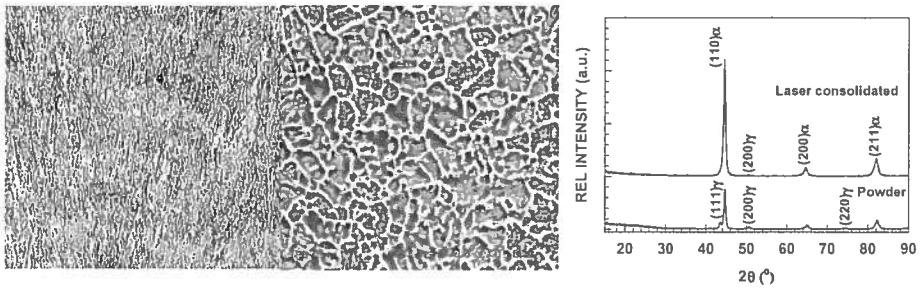

(a) (b) (c)

Fig. 4: Identification of microstructure and phase of LC H13 steel, (a) optical microscope observation along vertical cross-section, (b) SEM observation along horizontal cross-section, and (c) XRD patterns.

The XRD results indicated that the LC H13 steel consisted of a majority of α (martensite) plus trace amount of γ phase (Fig.4c), which was very similar to the H13 powder used for the consolidation with the exception of the reduced amount of γ phase. Further XRD analysis indicated that the carbides extracted from LC H13 material were of MC, M_7C_3 and possible M_3C types.

Table 2: Tensile properties of LC H13 tool steel.

Material Conditions		$\sigma_{0.2}$ (MPa)	σ_{UTS} (MPa)	E (GPa)	δ (%)
As-consolidated	Vertical	1288±54	2064±51	216±4	6.0±2.2
	Horizontal	1564±24	2033±38	214±2	5.0±2.8
Cast (annealed)[22]		370	670	-	Lower than wrought H13
Wrought (annealed) [23]		510	676	210	28
Wrought (1010°C/oil quench + 605°C tempering) [24]		1290	1495	-	15
Wrought (1010°C oil quench + 527°C tempering) [24]		1570	1960	-	13

The LC H13 tool steel showed excellent tensile properties (Table 2). The average yield and tensile strengths of the as-consolidated H13 along vertical direction were about 1288 MPa and 2064 MPa respectively, while the elongation was about 6% and the elastic modulus was about 216 GPa. Along the horizontal direction, the LC H13 showed significantly higher yield strength (1564 MPa) than along the vertical direction, while the tensile strength, elastic modulus and elongation of LC H13 were comparable for both directions. It should be noted that the tensile properties of the LC H13 material had relatively small scatter. For example, along the vertical direction, the standard deviations of the

yield strength and tensile strength were about 54 MPa and 51 MPa respectively, while the standard deviations of the elastic modulus and elongation were 4 GPa and 2.2% respectively, which indicated that the laser consolidated H13 material had a reasonably good consistency.

Compared to the conventional cast or wrought material, the LC H13 tool steel demonstrated excellent tensile properties. From the references [22-24], the yield and tensile strengths of the annealed cast or wrought H13 were about 370-510 MPa and 670 MPa respectively, while the yield and tensile strengths of the wrought H13 in hardened condition were in the range of 1290-1570 MPa and 1500-1960 MPa, respectively. The tensile and yield strengths of the as-consolidated H13 were substantially higher than the annealed cast or wrought H13, and comparable to the hardened wrought H13. The elastic modulus of the as-consolidated H13 was about the same as the wrought material. However, the elongation of as-consolidated H13 material was about 5-6%, which was lower than the hardened wrought H13. A post heat treatment might be used to improve the elongation of the LC H13 material if required.

The LC H13 showed very good wear resistance. The pin-on-disk wear test results indicated that, under the given test conditions (3.175 mm diameter Cr steel ball of Rc.63; 250g test load; total 4000 m sliding distance), as-consolidated H13 specimens showed significantly improved wear resistance as compared to hardened wrought H13 specimens. For example, the average volume loss of the as-consolidated H13 specimens was about 0.14 mm^3, which was only about 1/3 of the volume loss of the hardened H13 tempered at 482°C (0.4 mm^3) and about one order of magnitude less as compared to the annealed wrought H13 material (1.45 mm^3). In addition, the average wear volume loss of Cr steel balls tested against the LC H13 specimens (0.21 mm^3) was also significantly less (only 1/3 to 1/4) than that of the balls tested against the hardened or annealed wrought H13 specimens (0.56-0.88 mm^3).

Tool steel - CPM-9V

CPM-9V is a vanadium-carbide type of tool steel developed by Crucible Research for powder metallurgy applications. The CPM-9V powder contains 1.8% C, 9.26% V, 5.35% Cr, 1.24% Mo and 0.91% Si. Compared to conventional tool steels, CPM-9V exhibits excellent wear resistance [25].

The LC CPM-9V had a very fine microstructure, which was very hard to identify under optical microscope. A high resolution SEM photo (Fig.5a) showed that as-consolidated CPM-9V had two-phase microstructure: a light, very fine and snowflake-like phase precipitated on the dark matrix. The thickness of the light snowflake-like phase was only about 100 nm (Fig.5b). EDS analysis indicated that the light phase contained higher percentage of vanadium (about 12–14 %) and chromium (about 6–6.6%) as compared to the dark matrix (about 9% V and 5.7% Cr). The XRD analysis revealed that the light phase was $(V,Cr)_8C_7$ type carbides, while the dark portion was α phase.

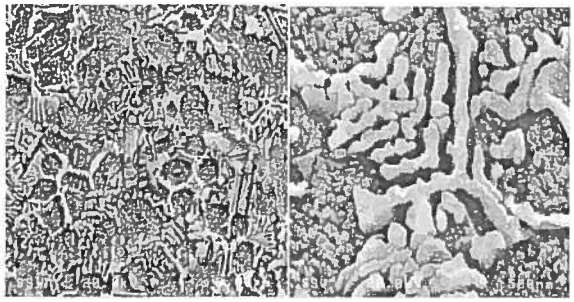

(a) (b)

Fig. 5: Microstructure of LC CPM-9V by high resolution SEM, (a) × 6,500, and (b) × 40,000.

Table 3: Tensile properties of LC CPM-9V tool steel

Sample No.	Vertical Direction (As-consolidated)			
	σ_{UTS} (MPa)	$\sigma_{0.2}$ (MPa)	δ (%)	E (GPa)
#1	1358.9	883.8	2.3*	229.6
#2	1295.0	787.0	2.8*	230.6
#3	1303.8	835.9	2.2*	244.5
#4	1303.8	778.1	3.1*	232.7
Average	**1315±29**	**821±49**	**2.6***	**234±7**

As-consolidated CPM-9V material showed good tensile properties (Table 3). Along the vertical direction, the as-consolidated CPM-9V had average yield strength of 821 MPa and tensile strength of 1315 MPa. The elastic modulus of the consolidated CPM-9V was about 234 GPa. Unfortunately, all specimens failed outside of the gauge length and therefore, the accurate elongation data were not available. But based on the measured data within the gauge length, the average elongation of the as-

consolidated CPM-9V would be 2.6% or higher. It should be noted that all tensile test data were very consistent and the scatter ranges were small, which again indicated that the laser consolidation process had good reproducibility.

LC CPM-9V also showed excellent wear resistance (Fig.6). Pin-on-disk wear test revealed that, under the given test conditions (WC ball of 6.375 mm diameter; 500g test load; total sliding distance of 8000 m), LC CPM-9V specimens (Rc.50-55) showed significantly better wear resistance as compared to hardened D2 (Rc. 64-65) and normalised 4340 (Rc.35-36) steels. The average volume loss of the LC CPM-9V specimens was about 0.0211 mm^3, which was only about the 1/3 of the volume loss of D2 specimens (0.0595 mm^3) and about one order of magnitude lower as compared to the 4340 specimens (0.2185 mm^3). In addition, the wear loss of WC balls tested against the LC CPM-9V material was also significantly lower than that of the same balls tested against the D2 and 4340 steel. The average wear volume loss of the WC balls against the LC CPM-9V was about 0.01855 mm^3, which was only about a half or one third of the ball volume loss against the D2 and 4340 steel (0.0417 mm^3 and 0.0538 mm^3), respectively. It is interesting to note that although the hardness of the LC CPM-9V material was only around Rc.50-55, but its wear resistance was clearly superior to the hardened D2 steel with a hardness of around Rc. 64-65, which was consistent with the observation on powder metallurgy (P/M) CPM-9V material [25]. The excellent wear resistance of the LC CPM-9V may be attributed to the precipitation of $(V,Cr)_8C_7$ carbides due to the high vanadium contents in the alloy.

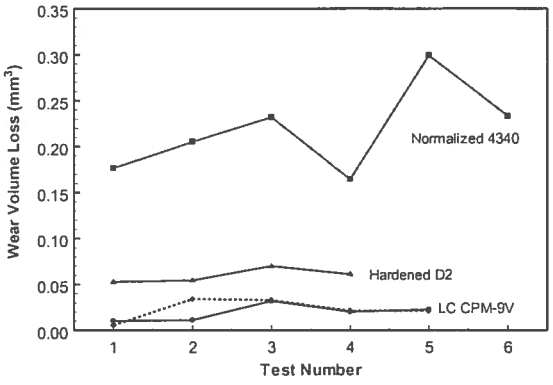

Fig. 6: Pin-on-disk wear test results (disk volume loss).

16.3.2 Ni-based alloys

IN-625 alloy

IN-625 is a nickel-base solution hardening superalloy and the powder used for laser consolidation contains 0.03% C, 22% Cr, 9% Mo, 3.7% Ta and Nb. Laser consolidation produced metallurgically sound IN-625 samples, free of cracks or porosity. The LC IN-625 material showed directionally solidified microstructure due to rapid solidification inherent to the process. The cross-sectional view along the vertical direction (build-up direction) reveals that columnar grains growing almost parallel to the build direction in the LC IN-625 (Fig.7a), while the horizontal cross section showed that the LC IN-625 consisted of fine cells of around 2-3 μm in diameter (Fig.7b). The XRD results revealed that the LC IN-625 had the same γ phase as the IN-625 powder: a face-centered cubic structure with a lattice parameter of 3.59 Å. The XRD results also revealed that the directional solidification of LC IN-625 material was along the (100) crystallographic plane, which was the typical dendritic growth direction of face-centered cubic structure materials.

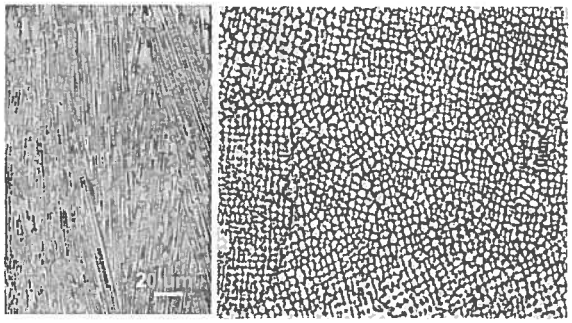

(a) (b)

Fig. 7: Microstructure of LC IN-625 alloy (a) vertical cross-sectional view, and (b) horizontal cross-sectional view.

Table 4: Tensile properties of LC IN-625 alloy

Conditions		$\sigma_{0.2}$ (MPa)	σ_{UTS} (MPa)	δ (%)
LC IN-625 (as-consolidated)	Horizontal	518±9	797±8	31±2
	Vertical	477±10	744±20	48±1
Cast IN-625 [26]		350	710	48
Wrought IN-625 [27]		490	855	50

The LC IN-625 material exhibited very good mechanical properties (Table 4). Along the horizontal direction (perpendicular to the build direction), the yield strength and tensile strength of the LC IN-625 material were 518 MPa and 797 MPa respectively, while the elongation was about 31%. When testing along the vertical direction (parallel to the build direction), both the yield and the tensile strengths were slightly lower to 477 MPa and 744 MPa respectively, while the percentage elongation increased significantly to 48%. The anisotropic behaviour of the tensile properties of the LC IN-625

alloy may be attributed to its directionally solidified microstructure. The yield strength and the tensile strength of the LC IN-625 along both directions were significantly higher than the cast material and comparable to the wrought IN-625, although the elongation along the horizontal direction was slightly lower [26-27].

IN-738 alloy

IN-738 is a nickel-base γ'-precipitation hardening superalloy. The powder we used contains 16.1% Cr, 8.34% Co, 3.27% Al, 3.38% Ti and other alloying elements. The alloy has excellent creep strength and hot corrosion resistance and has been used for manufacturing gas turbine airfoils in hot section [28]. Similar to the LC IN-625, the LC IN-738 also showed directionally solidified micro tru tur very fine columnar γ dendrites growing almost parallel to the building direction. XRD analysis revealed that the preferred orientation was along the (100) crystallographic plane. Precipitation of γ' particles is the primary strengthening mechanism for the IN-738 superalloy. The as-consolidated IN-738 material did not show γ'-precipitates, while precipitated carbides were distributed uniformly along the interdendritic regions. After a standard heat treatment cycle (1120°C × 2 hrs/air cooling + 845°C × 24 hrs/air cooling), a significant amount of γ'-particles precipitated in the LC IN-738 matrix (Fig.8a). Compared to the cast IN-738 (Fig.8b), the heat-treated LC IN-738 showed the similar but finer bimodal γ' distribution: coarse particles in near cuboidal shape plus fine particles.

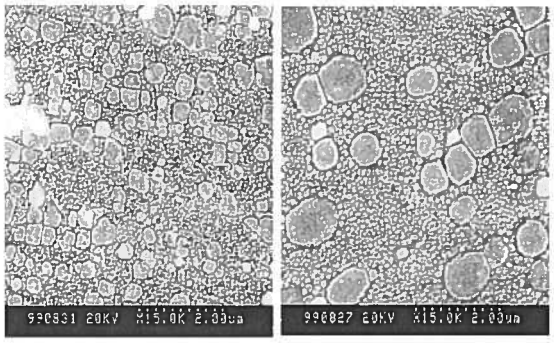

(a) LC IN-738 (b) Cast IN-738

Fig. 8: Observation of γ' precipitates in cast and LC IN-738, ×15,000.

Table 5: Tensile properties of LC IN-738 alloy

Material	Condition	σ_{UTS} (MPa)	$\sigma_{0.2}$ (MPa)	δ (%)
LC IN-738	Vertical direction (as-consolidated)	1202±23	869±5	18±2
	Vertical direction (heat-treated)	1269±35	869±19	17±2
	Horizontal direction (as-consolidated)	1084±23	880±14	6.7±1.7
Cast IN-738 [29]	Heat-treated	1100	915	5

The LC IN-738 material showed very good tensile properties (Table 5). Along the vertical direction, the tensile and the yield strength of the as-consolidated IN-738 was about 1202 MPa and 869 MPa respectively, while the elongation was about 18%. However, along the horizontal direction, the as-consolidated IN-738 showed comparable yield strength but relatively lower tensile strength and elongation as compared to the vertical direction. After the standard heat treatment, the tensile strength of the LC IN-738 along the vertical direction slightly increased to about 1269 MPa, while its yield strength and elongation remained almost the same. As compared to the heat treated cast IN-738 [29], the heat-treated LC IN-738 along the vertical direction showed 15% higher tensile strength and 240% higher elongation, although its yield strength was slightly reduced by about 5%.

Table 6: Stress rupture life of LC IN-738 tested at 1010°C (1850°F) and 55 MPa (8 ksi)

Sample No.	LC IN-738	LC IN-738/Cast IN-738	Cast IN-738 Baseline
#1	515 hrs.	123 hrs.	206 hrs.
#2	236 hrs.	175 hrs.	116 hrs.
#3	485 hrs.	128 hrs.	187 hrs.
#4	455 hrs.	-	-
Average	**423 hrs.**	**142 hrs.**	**170 hrs.**

The LC IN-738 material showed excellent stress rupture life (Table 6). Under the test condition (1010°C and 55 MPa), the average stress rupture life of LC IN-738 material was about 423 hours, which was more than double the life of the cast IN-738 baseline (170 hours). The excellent stress rupture life of the LC IN-738 may be attributed to its directionally solidified microstructure, uniform γ' particle precipitation, and fine and uniform carbide distribution.

16.3.3 Ti-base alloy

Ti-6Al-4V is an (α+β) titanium alloy that contains α stabilizer element Al and β stabilizer element V. The typical as-cast Ti-6Al-4V microstructure consists of transformed β containing acicular α as well as α at prior-β grain boundaries, while the annealed wrought Ti-6Al-4V bar typically consists of equiaxed α grain plus intergranular β [30]. The microstructure of the LC Ti-6Al-4V along the vertical

cross-section is shown in Fig. 9. The LC Ti-6Al-4V showed somewhat equiaxed grains (Fig.9a) with acicular phase inside (Fig.9b). A high-resolution SEM photo reveals that grain boundary was hard to distinguish and no secondary phase can be observed along it (Fig.9c).

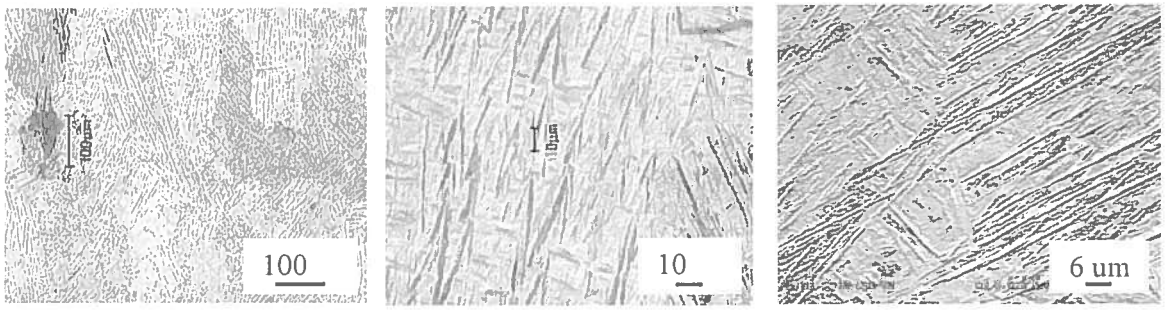

(a) Optical micrograph, ×100 (b) Optical micrograph, ×1000 (c) SEM micrograph, ×1500

Fig. 9: Microstructure of LC Ti-6Al-4V.

XRD results revealed that that wrought Ti-6Al-4V had majority of α phase plus small amount of β phase evidenced by the existence of β(200) peak. It is interesting to note that the LC Ti-6Al-4V and Ti-6Al-4V powder only had single α-phase microstructure with α(101) as the strongest diffraction peak without any β peaks, which was consistent with the optical microscope and SEM observations. The lack of β phase in LC Ti-6Al-4V and powder Ti-6Al-4V may also be attributed to the high cooling rate inherent to the process. Based on the optical microscope, SEM and XRD results, the LC Ti-6Al-4V microstructure consisted of somewhat equiaxed α grains (transformed from β) with acicular features inside.

Table 7: Tensile properties of LC Ti-6Al-4V alloy

Materials	$\sigma_{0.2}$ (MPa)	σ_{UTS} (MPa)	E (GPa)	δ (%)
As-consolidated Ti-6Al-4V (thick-wall specimens)	899	979	121	11.4
As-consolidated Ti-6Al-4V (thin-wall specimens)	1062	1157	116	6.2
Cast Ti-6Al-4V (As-cast or annealed) [31]	890	1035	-	10
Wrought Ti-6Al-4V (annealed bar) [32]	825	895	110	10
Wrought Ti-6Al-4V (solution treated and aged bar) [32]	965	1035	110	8
Wrought Ti-6Al-4V (solution heat treated + aged) [33]	1103	1172	-	10

The as-consolidated Ti-6Al-4V demonstrated excellent tensile properties (Table 7). The yield and tensile strengths of thin-wall (about 0.8 mm thick) LC Ti-6Al-4V were about 1062 MPa and 1157 MPa respectively, while its elongation was about 6.2%. The tensile and yield strengths of the as-consolidated thin-wall Ti-6Al-4V were substantially higher than the as-cast/annealed cast Ti-6Al-4V [31] and annealed wrought Ti-6Al-4V [32], and comparable to the wrought Ti-6Al-4V in solution treated plus aged condition [32-33]. The elastic modulus of the thin-wall LC Ti-6Al-4V (116 GPa) was comparable to the wrought material (110 GPa), although the elongation of the LC material (6.2%) was lower than the cast or wrought Ti-6Al-4V (8-10%). In other side, the as-consolidated thick-wall (about 1.5 mm thick) Ti-6Al-4V material was found to have a slightly lower tensile and yield strengths but a higher elongation than the thin-wall LC material. The average yield and tensile strengths of this material in the as-consolidated condition were 899 MPa and 979 MPa respectively, while the average elongation was around 11.4%. It should be noted that the tensile properties of as-consolidated thick-wall Ti-6Al-4V were vary comparable with the as-cast (or annealed) cast Ti-6Al-4V and annealed wrought Ti-6Al-4V material.

The LC Ti-6Al-4V also showed excellent bond strength to the wrought and laser-clad Ti-6Al-4V substrate. Under tensile testing at room temperature, the as-consolidated Ti-6Al-4V had average bond strength of about 1048 MPa to wrought Ti-6Al-4V substrate and about 1072 MPa to laser-clad Ti-6Al-4V substrate. It is interesting to note that all bond test specimens failed in the LC Ti-6Al-4V tube due to the stress concentration effect instead of at the bond area, which indicated that the actual tensile strength at the bond area was higher than the data obtained.

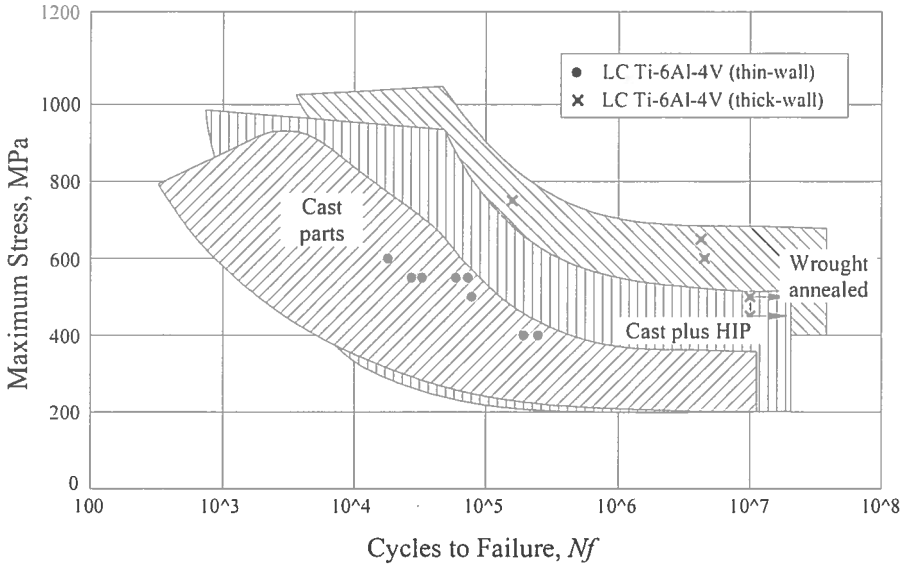

Fig. 10: Fatigue data of LC Ti-6Al-4V compared with cast and wrought/anneal Ti-6Al-4V (R=+0.1).

The as-consolidated Ti-6Al-4V also demonstrated excellent high-cycle fatigue properties (Fig.10). The plot also showed reference data [34] for cast, cast plus HIP and annealed wrought Ti-6Al-4V for comparison purposes. The endurance limit of the thin-wall (about 0.8 mm thick) LC Ti-6Al-4V specimens was around 400 MPa, which was at the high end of the scatter band of cast Ti-6Al-4V material. The endurance limit of the thick-wall (about 1.5 mm thick) LC Ti-6Al-4V material was in excess of 500 MPa, which was well at the high end of the scatter band of annealed wrought Ti-6Al-4V material. These preliminary results were very promising and demonstrated that the adjustment of LC processing parameters can significantly improve the fatigue properties of LC Ti-6Al-4V.

16.3.4 Co-base alloy

Stellite 6 is a Co-base wear resistant alloy containing 1% C, 27% Cr, 4.7% W and 0.9% Si. The Co-Cr-W system alloy retains its hardness at elevated temperatures and is especially effective for wear applications at high temperatures or in a corrosive environment, and are widely used as a wear-, corrosion- and heat-resistant material [35]. The LC Stellite 6 material showed a directionally solidified microstructure: very fine columnar dendrites growing almost parallel to the build vertical

direction (Fig.11). The details of the dendrite structure along the vertical cross-section were revealed by a high resolution SEM micrograph (Fig.11c). The dark regions were dendrite arms, while the interdendritic regions appeared white.

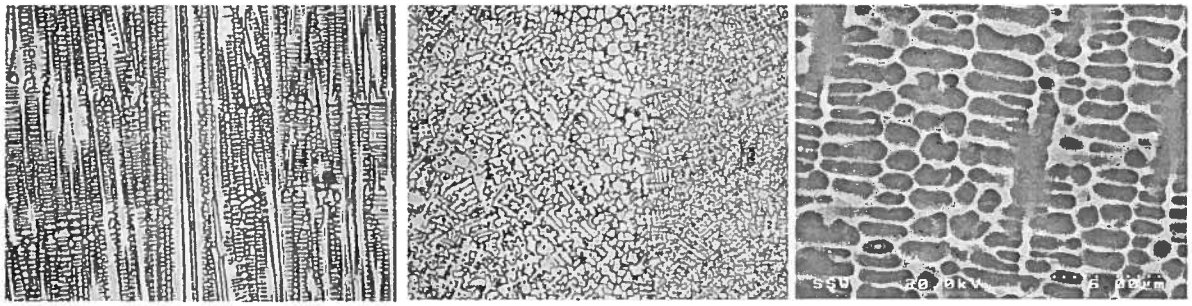

Fig. 11: Microstructure of the LC Stellite 6 material: (a) optical photo along vertical cross-section, ×1000, (b) optical photo along horizontal cross-section, ×1000, and (c) high magnification SEM photo along vertical direction, ×3300.

The average primary and secondary dendrite arm spacing (DAS) was measured to be around 3.3 μm and 1.2 μm respectively. X-ray energy-dispersive spectroscopy (EDS) results showed that chromium was enriched in the interdendritic regions (about 33-34%) as compared to about only 25-26% in the dendrite region. Due to the limitation of the EDS, carbon contents can not be determined. Based on the EDS results, it may be reasonable to deduce that chromium carbides were formed at the interdendritic regions in the LC Stellite 6. XRD results revealed that LC Stellite 6 material had the same phase as the Stellite 6 powder used for laser consolidation: cubic α phase. Preferred orientation along (100) plane was observed in the LC material, which was consistent with the optical microscope observation (Fig.11a). The carbides can not be detected by XRD technique due to their relatively small quantity.

Table 8: Tensile properties of LC Stellite 6 alloy

Processing Method	Condition	σ_{UTS} (MPa)	$\sigma_{0.2}$ (MPa)	δ (%)	HRc
LC Stellite 6	As-consolidated (Vertical)	1245±55	751±16	3.1±0.1	58
	As-consolidated (Horizontal)	1362±30	1023±15	3.2±0.4	59
Sand Casting [36]	Stress-relieved	834	541	1 - 2	46
Investment Casting [36]	As-cast	793	662	3	37
Powder Metallurgy [36]	-	896	-	<1	40

Compared to the conventional casting or powder metallurgy material, Stellite 6 produced using laser consolidation demonstrated significantly better mechanical properties: harder, stronger, and even more ductile (Table 8). The tensile strength of LC Stellite 6 was about 1245 MPa in the vertical direction and 1362 MPa in the horizontal direction, which were about 50% higher than that of the cast or powder metallurgy Stellite 6 (about 793 to 896 MPa) [36]. The yield strength of conventional cast and powder metallurgy Stellite 6 was about 541 to 662 MPa, while laser consolidation increased the yield strength to 751 MPa (vertical direction) and 1023 MPa (horizontal direction), representing an increase of 15-90%. The LC Stellite 6 material was also 25-55% harder than conventional Stellite 6. The average hardness of the LC Stellite 6 was about Rc 58 to 59, while only about Rc 37 to 46 was exhibited by the same material produced by the casting or powder metallurgy method. The elongation of LC Stellite 6 material was about 3.1-3.2%, which was similar to that obtained by investment casting (3%), but much better than that produced by sand casting (1-2%) or the powder metallurgy method (<1%).

The excellent mechanical properties of the LC Stellite 6 were attributed to its refined microstructure produced by the rapid solidification inherent to the laser consolidation process. It is well recognized that dendrite arm spacing (DAS) significantly affects the mechanical properties of cast alloys [37]. Generally speaking, an increase in the solidification rate reduces the DAS and results in increased mechanical properties [37]. The cooling rate during the conventional casting process is in the range of 10^{-3} – 1 k/sec, which results in a characteristic DAS of 50 to 500 μm. The characteristic DAS in the LC Stellite 6 material is only about 1.2 – 3.3 μm, which represents a cooling rate of 10^{3} – 10^{6} K/sec [38]. The fine DAS in the LC Stellite 6 directly contributes to its exceptional mechanical properties as compared to the conventional casting or powder metallurgy Stellite 6 material with a much coarser dendritic microstructure.

16.3.5 Al-base alloy

Al-Si alloys are one of the most important aluminium alloy systems, which possess medium strength, good flow characteristics, low melting point and narrow freeze range. Al 4047 is one type of Al-Si alloys and the powder used in this study contains 11.41% Si and 0.17% Fe. LC Al 4047 material showed a rapidly solidified microstructure with layered features: very fine columnar dendrites layer (almost parallel to the vertical build direction) growing on a layer of very fine equiaxed grains (Fig.12). The layered features may be attributed to the laser consolidation process itself. During the laser consolidation, the surface of previously deposited layer would be re-melted along with injected powder together and then re-solidified to form a new layer. Due to the high temperature gradient existed at the interface between the liquid layer and the previously deposited layer, a lot of nuclei formed on the most preferred seed sites - the previously deposited layer and grew into a layer of fine equiaxed grains. Then these grains further grew preferably along the direction of the maximum temperature gradient (parallel to the build-up direction) to form the columnar dendritic structure. Based on the high resolution SEM examination, LC Al 4047 material showed an average secondary dendrite arm spacing (DAS) of around 1-2 μm. Very fine cellular features were also observed along the transverse cross-section.

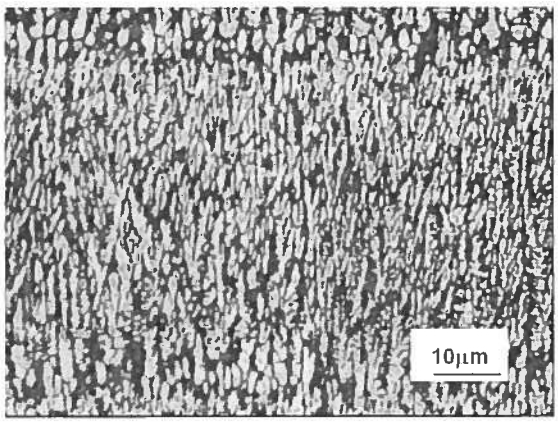

Fig. 12: Layer features observed in LC Al 4047 along vertical build-up direction.

The as-consolidated Al 4047 alloy showed very good tensile properties (Table 9). The average yield and tensile strengths of the as-consolidated Al 4047 were about 139 MPa and 317 MPa, respectively,

while the elongation was about 8.7% and the elastic modulus was about 74 GPa. All tensile test readings had small scatter, which indicated that the laser consolidation process had good reproducibility. As compared to tempered Al 4047 sheet material [39], as-consolidated Al 4047 showed about 70% higher tensile strength and about 3 times improved elongation, although its yield strength was about 24% lower.

Table 9: Tensile properties of LC Al 4047 alloy

Sample No.	$\sigma_{0.2}$ (MPa)	σ_{UTS} MPa)	δ (%)	E (GPa)
LC Al 4047 (as-consolidated)	**139±12**	**317±12**	**8.7±2.1**	**74±6**
Al 4047 sheet (tempered)[39]	184	197	3	-
Cast Al 413 (as-cast)[40]	145	300	2.5	-
Cast Al 443 (sand casting)[40]	55	130	8	71
Cast Al 443 (die-casting)[40]	110	230	9	71

Al 443 and Al 413 are two very important industrial cast Al-Si alloys. Al 443 contains 5.3% Si and is mainly used for sand castings and permanent mold castings. Al 413 is very similar to cast Al 4047 alloy, containing similar Si (11-13 %) but higher Fe (2 %). Al 413 is used to make various thin-walled and intricately designed castings. As-consolidated Al 4047 showed tensile and yield strengths very similar to as-cast Al 413 [40], but with substantially improved elongation (8.7% vs. 2.5%). Compared to both sand cast and die cast Al 443 alloy [40], as-consolidated Al 4047 showed much better yield and tensile strengths and comparable elongation. The elastic modulus of LC Al 4047 (74 GPa) was about the same as cast Al 443 (71 GPa). Unfortunately, elastic modulus of cast Al 413 can not be found in literatures for comparison.

16.4 Case studies of various industrial applications

16.4.1 Rotary cutting dies

Rotary cutting dies are a type of high-volume, high-speed tools used for cutting a wide range of materials (such as label, sand paper, carpet and fabric) from roll stocks, or directly in-line with

printing and processing equipment, resulting in a dramatic increase in the productivity and cost savings. The manufacturing of these rotary cutting dies, however, is costly and time-consuming. Depending on the complexity of the cutting pattern and the height of the cutting blades, the entire manufacturing process may take several days or even weeks to complete. The laser consolidation process provides unique capability to manufacture the rotary dies by building up cutting blades instead of machining them out from expensive tool steel stock. With this process, more wear resistant materials can be used to build up the cutting blades on a low cost blank without the need of heat treatment. Even further, the cutting blades on the used or damaged cutting dies can be easily machined away and the die blank can be reused to build new cutting dies. Thus, the consolidation process could significantly reduce the lead-time in the manufacturing of cutting die along with an improved life and reduction of its production cost. In collaboration with Rotoflex International, NRC-IMI investigated laser consolidation of CPM-9V for manufacturing cutting blades on low-cost substrate [15].

Dimensional accuracy measurements

A rectangular cutting pattern built up by the laser consolidation of CPM-9V on a flat base was used for the dimensional accuracy measurement (Fig.13). Results showed that the distance between the opposite walls was very uniform (Table 10). The standard deviation of the three measurements for distance L1 and L2 was only about 0.028 mm and 0.005 mm respectively, and the difference between the actual built wall and the desirable CAD design was only about 0.030 mm for both cases. Through-wall thickness was also very uniform with a standard deviation from 0 to 0.046 mm. However, there was slightly more thickness difference between different walls. The thickness of the thickest wall D was about 1.153 mm, while the thinnest wall C was only about 0.927 mm, leaving the maximum thickness difference between the walls to about 0.226 mm. Since all laser-consolidated walls will be machined to final dimension, such a thickness difference will not affect the sharpening of the cutting blades as long as the distance between walls and the through-wall thickness leave enough tolerance for the final finish machining.

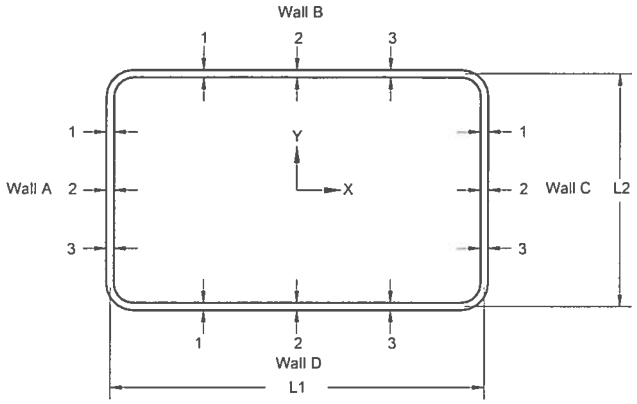

Fig. 13: Details of dimensions taken for measurements on a laser consolidated rectangular cutting pattern.

Table 10: Dimensional measurement of laser-consolidated cutting pattern

Dimension	Measurements (mm)			Avg. (mm)	Std. Deviation (mm)	Nominal (mm)	Diff. (mm)
	Pos. 1	Pos. 2	Pos. 3				
Wall Thickness Measurement							
Wall A	0.996	1.034	1.036	1.021	0.023	-	-
Wall B	1.143	1.143	1.143	1.143	0.000	-	-
Wall C	1.001	1.008	0.927	0.978	0.046	-	-
Wall D	1.153	1.146	1.153	1.151	0.005	-	-
Wall Distance Measurement							
L1	50.744	50.764	50.800	50.770	0.028	50.800	-0.030
L2	31.463	31.463	31.471	31.466	0.005	31.496	-0.030

Production testing

Various types of rotary cutting dies have been successfully made by using laser consolidation process to build CPM-9V cutting blades on low cost blank. Fig. 14 demonstrated a laser consolidated rotary cutting die after the final sharpening. Field production testing showed that the LC CPM-9V rotary cutting dies had successfully cut more than 180,000 meters of labels without re-sharpening, while the dies made by D2 tool steel usually need re-sharpening after running the same period.

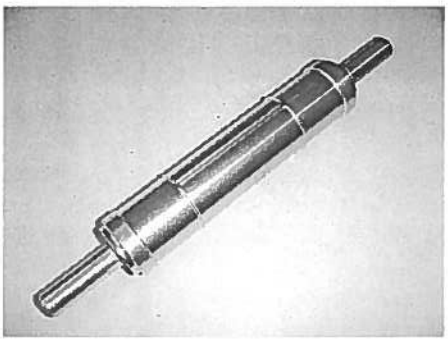

Fig. 14: Laser-consolidated CPM-9V rotary cutting die after a final sharpening

Based on our industrial partner's estimation, the laser consolidation process has the potential to manufacture rotary cutting dies with reduced manufacturing time by 1/3 (for dies larger than 5" dia.), reduced material cost by approximately 50% and increased cutting die life by approximately 100%. In addition, with this process, worn cutting blades could be repaired or the same blank could be reused for building a new cutting pattern after machining out the old pattern - recycling die blanks to reduce environmental impact.

16.4.2 Airfoils with embedded cooling channels

NRC-IMI worked with GE Global Research to explore the potential application of the laser consolidation of Ti-6Al-4V alloy to produce advanced gas turbine airfoil that contains complex geometric features that may be very difficult or even impossible to manufacture using other conventional manufacturing methods [16].

To test the capability of the laser consolidation process, an airfoil with embedded cooling channels was designed. It had a double-walled shape with seven bridges connecting two walls to provide structural integrity. The wall thickness of the inner and outer walls of the airfoil was about 0.762 mm, while the gap between the two walls was approximately 0.635 mm. The overall length of the airfoil was 33.02 mm and its overall width was around 10.16 mm. The height of the airfoil was set to 25.4 mm. The airfoil design containd many complex internal features such as sharp corners and relatively

narrow gaps that extended throughout the body of the airfoil. These features would be very difficult if not impossible to produce using conventional manufacturing methods. The airfoil design provided a good technical challenge for laser consolidation process.

Using optimized processing methodology and laser path planning strategy, laser consolidation successfully built the net-shaped Ti-6Al-4V airfoils of about 25.4 mm in height as per the design (Fig.15). The airfoil with embedded cooling channels was in the "as-consolidated" surface condition without further operation except grinding of the top surface. The laser consolidation process demonstrated the unique manufacturing capability to produce functional net-shape components. The combination of the innovative design with the unique capability of the LC process can lead to the creation of components with highly complex geometry not possible with conventional means.

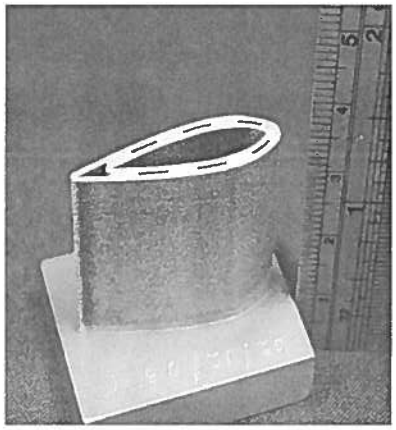

Fig. 15: Demonstration piece of the complex LC Ti-6Al-4V airfoil.

16.4.3 Net-shape functional sonar shells

The folded shell projector (FSP) is a compact flextensional sound source being developed by the Defense Research & Development Canada (DRDC) for low frequency sonar applications. The FSP radiates sound from a thin-walled cylindrical shell driven by a piezoelectric or magneto-strictive motor. The shell has superimposed corrugations (Fig.16a), which creates a significant challenge for the existing manufacturing technology. In collaboration with DRDC, NRC-IMI investigated laser consolidation of IN-625 and Ti-6Al-4V alloys for manufacturing net-shape functional FSP shells for refining the FSP design as well as for field testing [17].

LC IN-625 FSP shells

A CAD drawing of a FSP shell and an as-consolidated IN-625 FSP shell of the design after removing the loose powder are shown in Fig.16 (a) and (b). The shell is about 130 mm in height and around 80 mm in diameter. It is evident that the as-consolidated shell showed very good surface finish. A magnified cross-sectional view (Fig.16c) reveals that the laser consolidation process successfully manufactured the complex thin wall structure with excellent uniformity. It also showed that, as per the CAD design requirement, the laser consolidation process managed to generate a sharp corner inside each crest, which was very difficult to form using conventional manufacturing methods.

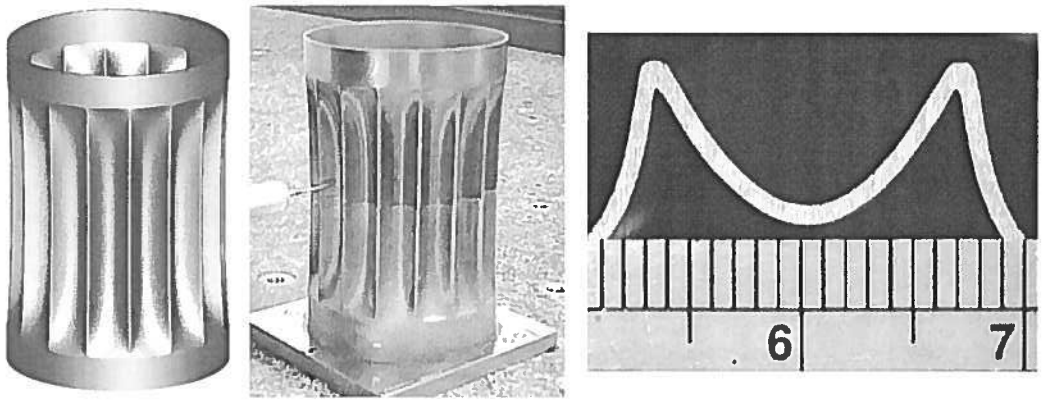

(a) (b) (c)

Fig. 16: FSP shell of one design, (a) CAD drawing, (b) LC IN-625 shell, and (c) magnified cross-sectional view of crests on the half shell.

In order to ensure the quality of the LC IN-625 shells, strict NDT inspections were performed on the LC shells by using ultrasonic, dye penetrant, X-ray and magnetic methods. The NDT inspection results revealed that the LC IN-625 shells were metallurgically sound, without porosity, cracks or other detectable defects. The functional testing performed by DRDC on the folded shell projectors assembled with LC IN-625 shells demonstrated that the resonance frequency of the sonar devices matched excellently with the design prediction from DRDC's finite element model.

LC Ti-6Al-4V FSP shells

A Ti-6Al-4V version of the FSP was designed by DRDC and manufactured by NRC-IMI. The shell is about 130 mm in height and around 55 mm in diameter. The surface uniformity of the LC Ti-6Al-4V shell was further improved and the line in the middle of the original LC IN-625 shell was eliminated (Fig.17). Visual inspection and acoustic testing revealed that all shells were metallurgically sound, without any cracks or visible defects. The dimensions of external fold profiles of Ti-6Al-4V FSP shells were inspected using a Brown & Sharpe Coordinate Measuring Machine (CMM) at 7 elevations [17]. The CMM probing path was created using Unigraphics to guide the measurement. The measurement results revealed that the LC Ti-6Al-4V FSP shell had an average deviation of 0.098 mm as compared with the CAD model with a minimum deviation of -0.282 mm and a maximum deviation of 0.177 mm. The diameter and wall thickness of the upper and lower flanges were measured using a micrometer with a ball end. The diameters of upper and bottom flanges were 54.501 mm and 54.606 mm respectively, while CAD model required 54.60 mm. The roundness was about 0.030 mm and 0.044 mm for upper and bottom flanges respectively. The CAD model specified a wall thickness of 0.80 mm, while the measurement showd that the upper and bottom flanges had the same wall thickness of 0.864 mm. It is evident that the LC Ti-6Al-4V shell demonstrated excellent dimensional accuracy.

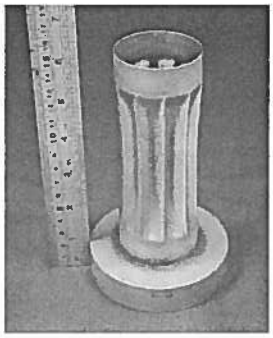

Fig. 17: LC Ti-6Al-4V FSP shell.

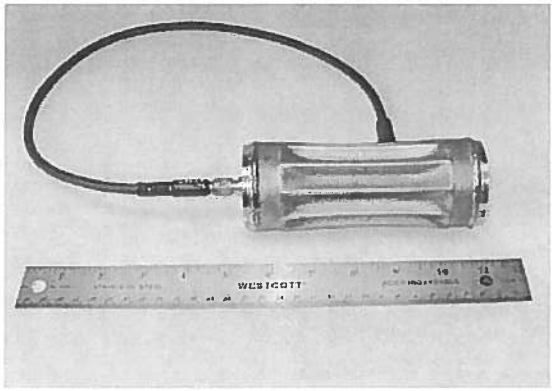

Fig. 18: Assembled LC Ti-6Al-4V FSP with welded Ti end caps

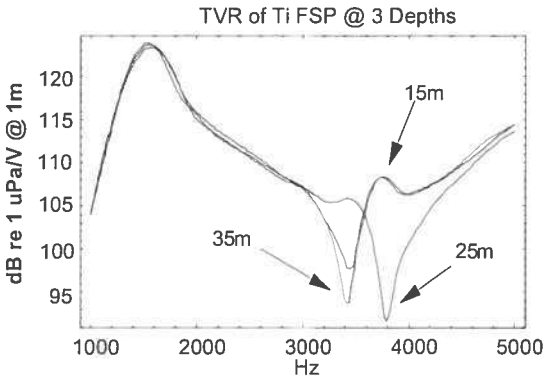

Fig. 19: Field testing results of LC Ti-6Al-4V FSP with welded Ti end caps.

Fig.18 illuminates a completed LC Ti-6Al-4V FSP assembly, while Fig.19 shows its field testing results. It has been proven that the welded LC Ti-6Al-4V FSP met its design goals of resonant frequency, source level and insensitivity to depth. The LC Ti-6Al-4V FSP was calibrated at depths of 15 m, 25 m and 35 m, showing identical resonant frequency of 1500 Hz.

In collaboration with DRDC, the laser consolidation process has been successfully utilized to manufacture seven Ti-6Al-4V and ten IN-625 complex FSP shells of four different designs and, at this moment, it is the only proven manufacturing technology to make functional net-shape FSP shells for field testing.

16.4.4 Structural components for ARMS

Through the Advanced Robotic Mechatronics System (ARMS) project in collaboration with MD Robotics and Canadian Space Agency, NRC-IMI investigated laser consolidation as a rapid functional prototyping method for making Ti-6Al-4V structural components for the system [18]. One goal of the ARMS project was to develop a multifunctional structure capable of providing high structural stiffness, with dedicated features to support electronic driver/control cards and the data/power bus while allowing the dissipation of the heat generated by the electronic drivers. The laser consolidation process was successfully used to build functional demonstration pieces for the various designs as well as the final test-pieces of the multifunctional boom. Fig. 20 shows a Ti-6Al-4V boom built using the

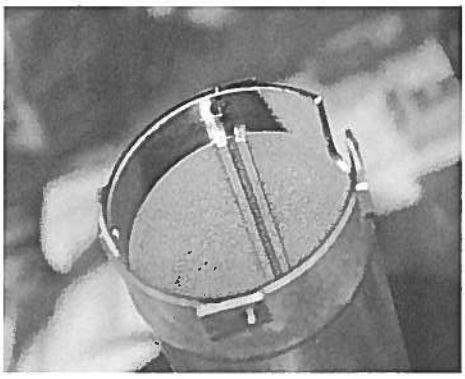

Fig. 20: LC Ti-6Al-4V boom with a slot to hold electronic card, after final machining.

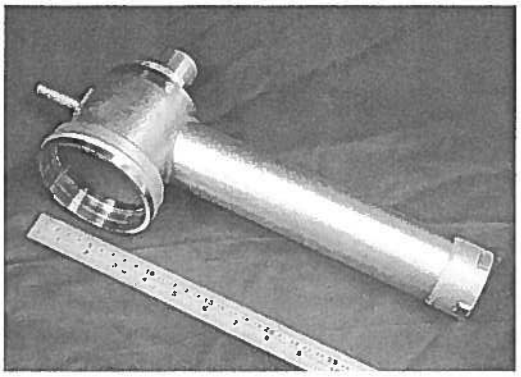

Fig. 21: LC Ti-6Al-4V integrated boom/housing, after initial machining.

laser consolidation process. The boom had four ribs forming a slot to hold electronic card. The LC Ti-6Al-4V boom was used in as-consolidated surface finish, except the contact surfaces that were machined for assembling.

Conventional design of a space robot manipulator generally consists of separate booms and joint housings that are connected to each other through a flanged interface, which substantially increases the weight and complexity. One-piece integrated boom/housing design is preferable to reduce the weight, complexity and increasing interface stiffness of a typical robotic arm. However, it is extremely difficult or even impossible to make the one-piece integrated boom/housing using conventional manufacturing processes. The LC process is a free-form fabrication process that allows the building of net-shaped functional features on existing components. Therefore, it offers the unique capability to build multi-functional boom on pre-built housing to realize the innovative design for one-piece integrated boom/housing. Fig. 21 shows an integrated boom/housing manufactured using laser consolidation of Ti-6Al-4V alloy. The integrated LC Ti-6Al-4V boom/housing showed as-consolidated surface finish, except the contact surfaces that were initially machined for next stage final machining and assembling.

Laser consolidation process successfully built multi-functional boom, housings #1 with interface, and housing #2 with integrated boom. The ARMS prototype robotic joint was assembled by MD Robotics

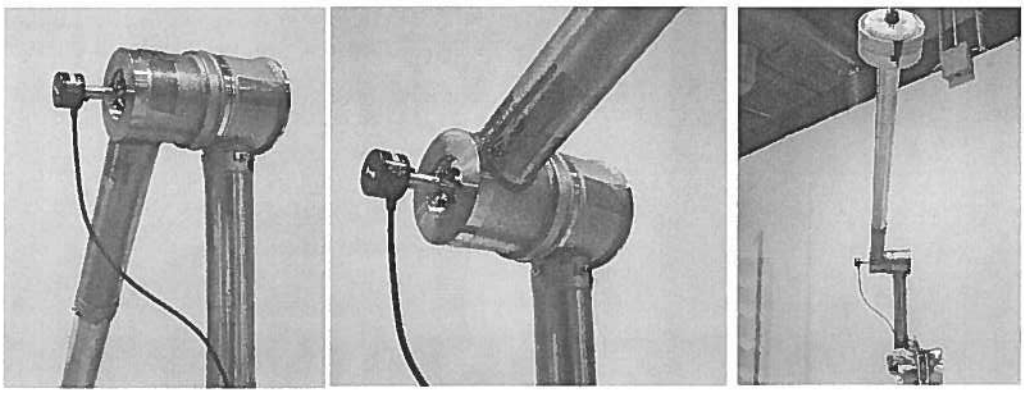

(a) (b) (c)

Fig. 22: Assembled ARMS with LC Ti-6Al-4V structural components, (a) and (b) close views, and (c) testing with payload.

using the LC Ti-6Al-4V structural components along with the other mechanical and electronic components. Fig.22 (a) and (b) show a close view of the assembled joint, while Fig. 22 (c) shows the ARMS with required payload during laboratory testing. The real time testing results demonstrated that the laser-consolidated components performed very well and all design requirements such as low weight and high strength were achieved.

16.4.5 Functional net-shape components for potential rocket engine applications

Design and manufacturing of rocket engines requires the manufacturing of various small quantity but complex shaped components. Laser consolidation process provides unique capability to manufacture these small quantity functional components to shorten the manufacturing cycle and to reduce (or even eliminate) tooling cost. NRC-IMI worked with Pratt and Whitney Rocketdyne (PWR) to explore the laser consolidation process for manufacturing functional net-shape components as well as tooling for potential rocket engine applications [19].

LC IN-625 demonstration pieces

An IN-625 part was initially designed to demonstrate the capability of the laser consolidation process (Fig.23a). It consists of 5 portions: (a) cylinder #1 (3 mm thick), (b) cylinder #2 (2 mm thick), (3) a conical top on a short cylinder (0.81 mm thick), (4) a circular fin (2 mm thick), and (5) substrate disk (50 mm in diameter and 9.4 mm thick). Laser consolidation of IN-625 was performed with a 5-axis

motion system to build the demonstration piece on a 1020 steel substrate. A hole with a diameter of 8 mm was pre-drilled in the middle of the substrate to allow the release of the loose powder inside the part after laser consolidation. The steel substrate formed the part of the final demonstration piece. Fig. 23 (b) shows the as-consolidated IN-625 demonstration piece after removing the loose powder. It is evident that the as-consolidated part showed very good surface finish.

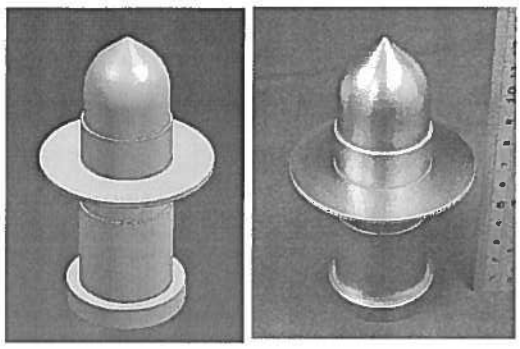

(a) (b)

Fig. 23: IN-625 demonstration piece with conical top, (a) CAD drawing and (b) LC part.

The cross-sectional view of the part (Fig.24a) reveals that, as per the CAD design requirement, the laser consolidation process managed to build the LC IN-625 conical top with very uniform wall thickness and the tip was sealed very well. Fig. 24(b) shows that all four sections of the LC IN-625 piece demonstrated uniform wall thickness. Detailed examination of the cross-section further revealed that all four portions of the LC IN-625 demonstration piece were metallurgically sound, without cracking or porosity. The bonding between sections and to substrate plate was excellent.

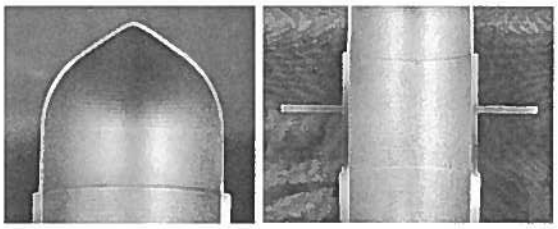

(a) (b)

Fig. 24: Cross-section of LC IN-625 demonstration piece, (a) conical top and (b) middle section.

Dimensions measurement revealed that the internal diameter of the LC IN-625 part was 38.15 mm, which was only 0.05 mm larger than the design. The thickness of the conical top was 0.81 mm, exactly the same as per the design. The thickness of the cylinder was about 0.15 mm thicker than the design, which may be attributed to the deviation in arranging existing multi-pass to fit the required thickness and can be improved in the future.

LC Ti-6Al-4V spherical hollow ball

One of the demonstration pieces is a spherical hollow ball made of Ti-6Al-4V. The ball requires an outside diameter of 51.501 mm with a deviation of +/- 0.254 mm and a wall thickness of about 0.7 mm. The ball needs to be fully sealed without any unfinished pores or leaks. The Ti-6Al-4V hollow ball is usually manufactured by forming two halves of the ball separately through machining, forming or other appropriated methods and then welding them together, which involves many manufacturing steps. For high end users, the thickness uniformity of the ball, especially at the weld area is always a big concern.

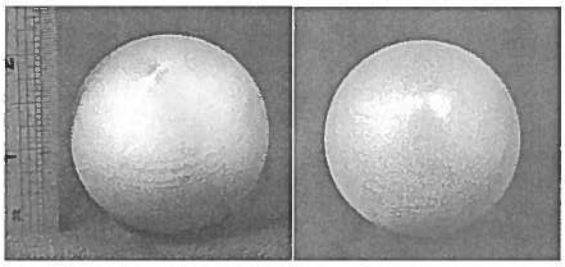

(a) (b)

Fig. 25: LC Ti-6Al-4V hollow ball, (a) top view, and (b) bottom view.

As a rapid manufacturing process, laser consolidation process provides the possibility to build the spherical hollow ball directly. However, there is no reference available regarding other similar processes to build spherical hollow ball directly from Ti-6Al-4V powder. Laser consolidation was investigated to build the entire functional net-shape spherical hollow ball from Ti-6Al-4V powder in one step to demonstrate its processing capability. A 5-axis motion system was used for this work. A special laser consolidation procedure was developed to build the ball from a Ti-6Al-4V substrate and to close it at the top. After laser consolidation, the ball was machined off from the substrate.

Fig. 25(a) shows a top view of the as-consolidated ball after removing loose powder. It is evident that the as-consolidated Ti-6Al-4V ball showed reasonably good surface finish. Especially, it revealed that laser consolidation process successfully closed the hollow ball without any defects. Fig. 25(b) shows a bottom view of the ball, which reveals that a small portion of the substrate formed the part of the final ball after being cut off from the substrate.

The outside diameters of the LC Ti-6Al-4V ball were measured using a Mitutoyo Precision Height Gauge, 45° apart along both polar and equatorial orbits, and data were listed in Table 11. The measurements were compared with the nominal diameter from the CAD model of the ball and the deviation was calculated for each measurement. Based on the CAD data, the outside diameter of the ball should be 51.501 mm. The measurement of the LC Ti-6Al-4V ball along polar orbit showed the maximum diameter of 51.575 mm and the minimum diameter of 51.397 mm. Along equatorial orbit, all the measurements were the same (51.575 mm in diameter), which demonstrated excellent uniformity of the ball.

Table 11: Measurement of Outsider diameters of LC Ti-6Al-4V ball (mm)

Angle	Measurement	CAD	Deviation
Measured in polar orbit			
0°	51.575	51.501	+0.074
+45°	51.486	51.501	-0.015
+90°	51.397*	51.501	-0.104*
-45°	51.473	51.501	-0.028
Measured in equatorial orbit			
0°	51.575	51.501	0.074
+45°	51.575	51.501	0.074
+90°	51.575	51.501	0.074
-45°	51.575	51.501	0.074

It is obvious that the LC Ti-6al-4V ball showed excellent dimensional accuracy. The deviation of outsider diameter of the LC Ti-6Al-5V ball was in the range of +0.074 mm and -0.104 mm, which was significantly less than the required deviation of +/-0.254 mm. If disregard the (*) data that was affected by the cut-off process, the deviation will be even smaller (+0.074 mm and -0.028 mm).

16.5 Future trend of the technology

As demonstrated in the previous sections of the chapter, laser consolidation process provides the unique capability to produce net-shape functional components directly from CAD models without moulds or dies, which enables the rapid manufacturing of small quantity metallic components with short delivery time and reduced production cost. However, this technology is still emerging and much more developmental work is needed.

It is expected that more industrial materials will be investigated using the laser consolidation process. A comprehensive database of laser consolidated materials, its microstructure, mechanical and other properties will be generated through collaboration among research organizations, universities and industries. The processing capability of the technology will be further improved to build more complex net-shape functional components that can not be produced currently. The processing speed will be substantially improved to meet industrial needs for production. The adoption of advanced sensing and control capability and software development will further improve the robustness of the process in the production environment.

With the increased interest from various industries, it is expected that more industrial applications will be developed, especially in the fields of aerospace, medial devices and tooling. In combination with innovative design, the laser consolidation process along with 5-axis CNC motion system provides unique capability to produce complex components with delicate details that are very difficult or even impossible to make using conventional manufacturing processes. In combination with other manufacturing technologies, laser consolidation can build integrated delicate features on components manufactured using conventional low cost methods. Compared to traditional welding process, the heat input induced by the laser consolidation process to the substrate is minimal. Therefore, laser consolidation process also provides the possibility to build unique features on thin-walled components to provide additional functionality, reduce manufacturing time and cost. In addition, since laser consolidation does not require any moulds or dies, it provides the possibility to design and manufacture components directly through internet to combine the real strength of virtual manufacturing and rapid manufacturing. It also provides the flexibility to change the design quickly to make functional components to meet various industrial demands to produce customized components with significantly reduced lead-time. It is expected that this computer aided manufacturing (CAM) technology will make a huge impact on manufacturing in a wide range of industries in the near future.

Acknowledgement

The author would like to thank Andre Theriault, Yangsheng Li, Jianyin Chen, Sheng-hui Wang, Glen Campbell, Allan Gillett, Gary Wabersich, Nelson Santos, Brian Gibson, Jon Fenner and Mike Meinert for their numerous contributions in process development, sample preparation and characterization. Thanks are also due to M.U. Islam for his many valuable discussions during various projects.

16.6 References

[1] O. Milewski, G.K. Lewis, D.J. Thoma, J.I. Keel, R.B. Nemec and R.A. Reinert, "Directed Light Fabrication of A Solid Metal Hemisphere Using 5-Axis Powder Deposition", Journal of Materials Processing Technology, **75**, pp.165-172 (1998).

[2] D.M. Keicher, W.D. Miller, J.E. Smugeresky and J.A. Romero, "Laser Engineering Net Shaping (LENS™): Beyond Rapid Prototyping to Direct Fabrication", Proceedings of the 1998 TMS Annual Meeting, pp.369-377 (1998).

[3] M.A. McLean, G.J. Shannon and W.M. Steen, "Laser Generating Metallic Components", Proceedings of the SPIE, **3092**, pp.753-756 (1997).

[4] D.J. Thoma, C. Charbon, G.K. Lewis and R.B. Nemec, "Directed Light Fabrication of Iron-Based Materials", Materials Research Society Symposia Proceedings, **397**, pp.341-346 (1996).

[5] D.J. Thoma, G.K. Lewis and R.B. Nemec, "Solidification Behavior During Directed Light Fabrication", Proceedings of the 2nd International Conference on Beam Processing of Advanced Materials, pp.247-253 (1995).

[6] F. Klocke, H. Wirtz and W. Meiners, "Direct Manufacturing of Metal Prototypes and Prototype Tools", Proceedings of Solid Freeform Fabrication Symposium, pp.141-148 (1996).

[7] G.A. Whitlow and G.J. Bruck, "Laser Beam Casting of Metal Powder into Near Net Shape Products", Power Beam Processing: Electron, Laser, Plasma-Arc: Proceedings of the International Power Beam Conference, pp.207-210 (1988).

[8] Sandia National Laboratories, "Creating a Complex Metal Part in a Day is Goal of Commercial Consortium", news release on Sandia National Laboratories' web site: http://www.sandia.gov/media/lens.htm (December 4, 1997).

[9] L. Xue, M.U. Islam, "Free-Form Laser Consolidation for Producing Metallurgically Sound and Functional Components", Journal of Laser Applications, 12(4), 2000, pp.160-165.

[10] L. Xue, J.-Y. Chen and M.U. Islam, "Functional Properties of Laser Consolidated Wear Resistant Stellite 6 Alloy", Powder Metallurgy Alloys and Particulate Materials for Industrial Applications, ed. by David E. Alman and Joseph W. Newkirk, pp.65-74, 2000.

[11] L. Xue, J.-Y. Chen, M.U. Islam, J. Pritchard, D. Manente and S. Rush, "Laser Consolidation of IN-738 Alloy for Repairing Cast IN-738 Gas Turbine Blades", Proceedings of 20th ASM Heat Treating Society Conference, St.-Louis, Missouri, USA, October 8 – 12, 2000, pp.1063-1071.

[12] L. Xue, J.-Y. Chen, A. Theriault, "Laser Consolidation of Ti-6Al-4V Alloy for the Manufacturing of Net-Shape Functional Components", Proceedings of 21st International Congress on Applications of Lasers and Electro-Optics (ICALEO 2002), Scottsdale, USA, 2002, pp.169-178.

[13] L. Xue, J.-Y. Chen, A. Theriault, "Laser Consolidation of Al 4047 Alloy", Proceedings of 24th International Congress on Applications of Lasers and Electro-Optics (ICALEO 2005), Miami, USA, 2005, pp.344-351.

[14] L. Xue, A. Theriault, S-H. Wang and J. Chen, "Laser Consolidation of Functional Shell Structure", Proceedings of the 5th International Workshop on Advanced Manufacturing Technologies (AMT 2005), London, Ontario, Canada, 2005, pp.231-236.

[15] L. Xue, A. Theriault, J. Chen, M.U. Islam, A. Wieczorek and G. Draper, "Laser Consolidation of CPM-9V Tool Steel for Manufacturing Rotary Cutting Dies", Proceedings of 10th International Symposium on Processing and Fabrication of Advanced Materials, 2001 ASM Materials Solution Conference and Exposition, Indianapolis, Indiana, USA, November 5-8, 2002. pp.361-376.

[16] L. Xue, A. Theriault, M.U. Islam, M. Jones, H.P. Wang, "Laser Consolidation of Ti-6Al-4V Alloy to Build Functional Net-Shape Airfoils with Embedded Cooling Channels", Proceedings of the 23rd International Congress on Applications of Lasers and Electro-Optics (ICALEO' 2004), San Francisco, California, USA.

[17] L. Xue & C. Purcell, "Laser Consolidation of Net-Shape Shells for Flextensional Sonar Projectors", Proceedings of the 25th International Congress on Applications of Lasers and Electro-Optics (ICALEO 2006), Scottsdale, Arizona, USA, pp.686-694.

[18] L. Xue, A. Theriault, et al., "Investigation of Laser Consolidation Process for Manufacturing Structural Components for Advanced Robotic Mechatronics System", Proceedings of 22nd International Congress on Applications of Lasers and Electro-Optics (ICALEO 2003), Jacksonville, Florida, USA, 2003, pp.134-143.

[19] L. Xue, Y. Li, T. Van Daam & C. Bampton, "Investigation of Laser Consolidation for Manufacturing Functional Net-Shape Components for Potential Rocket Engine Applications", Proceedings of the 26th International Congress on Applications of Lasers and Electro-Optics (ICALEO 2007), Orlando, Florida, USA, pp.161-169.

[20] ASM International, *Metals Handbook*, Ed. 9. Vol. 3. (ASM International, Ohio, 1980), p.113.

[21] ASM International, *Metals Handbook*, Ed. 9. Vol. 3. (ASM International, Ohio, 1980), p.21.

[22] Micronalloys, 2002, Information provided through an e-mail.

[23] http://www.moldsteel.com.

[24] ASM International, 1990, *Metals Handbook*, Vol. 1, pp.442.

[25] K.E. Pinnow and W. Stasko, "P/M Tool Steel", Metals Handbook, 10th edition, Vol.1, ASM International, Ohio, pp.786-789, 1990.

[26] G.L. Erickson, "Polycrystalline Cast Superalloys", Metals Handbook 10th Edition, Vol.1, ASM International, Ohio, p.984, 1990.

[27] F.R. Morral, "Wrought Superalloys", Metals Handbook, 9th Edition, Vol.3, American Society for Metals, Ohio, p.219, 1980.

[28] ASM Committee on Cast Corrosion–Resisting and Heat-Resisting Alloys, "Heat-Resistant Casting", Metals Handbook, 9th Edition, Vol.3, American Society for Metals, Ohio, pp.278, 1980.

[29] ASM Handbook Committee, "Properties of Superalloys", Metals Handbook, 9th Edition, Vol.3, American Society for Metals, Ohio, pp.244-245, 1980.

[30] Boyer, R.R., 1985, "Titanium and Titanium Alloys", ASM Handbook, Vol.9: Metallography and Microstructures, ASM International, pp. 458-475.

[31] Newman, J.R., 1980, "Titanium Castings", Metals Handbook 9th Edition, Vol. 3, American Society for Metals, pp.409.

[32] ASM Committee on Titanium and Titanium Alloys, 1980, "Properties of Titanium and Titanium Alloys", Metals Handbook 9th Edition, Vol. 3, American Society for Metals, pp.388-389.

[33] Davis, J.R., 1997, "Titanium and Titanium Alloys", ASM Specialty Handbook: Heat-Resistant Materials, ASM International, pp.347-360.

[34] Eylon, D., Newman J.R. and Thorne J.K., 1990, "Titanium and Titanium Alloy Castings", ASM Handbook, Vol.2: Properties and Selection: Nonferrous Alloys and Special-Purpose Materials, ASM International, p. 642.

[35] Paul Crook, "Cobalt and Cobalt Alloys", ASM Handbook, Vol.2, ASM International, Ohio, pp.446-454, 1990.

[36] Data supplied by Deloro Stellite Inc., June 1999.

[37] M.C.Flemings, "Solidification Processing", McGraw-Hill Book Company, New York, pp.342-343, 1974.

[38] D.Apelian, "Solidification Mechanics and Mechanism", Encyclopedia of Materials Science and Engineering, Vol. 6, Pergamon Press, New York, pp.4525-4529, 1986.

[39] Eagle Alloys Group (2005) Mechanical testing data for Al 4047 sample material.

[40] Kearney, A.L. (1990) Properties of Cast Aluminum Alloys, in ASM Handbook Volume 2: Properties and Selection: Nonferrous Alloys and Special-Purpose Materials, ASM International, 171-173.

[41] Bampton, C., Goodin, W., Van Daam, T., Creeger, G. & James, S. (2005) Net-Shape HIP Powder Metallurgy Components for Rocket Engines, in Proceedings of 2005 International Conference on Hot Isostatic Pressing, Paris, France, pp. 53.

[42] Samarov, V. (2006) HIP of Net Shape Parts for Critical Applications from Advanced Powder Materials, in Proceedings of NATO AVT-139 Specialists' Meeting on Cost Effective Manufacture via Net Shape processing, Amsterdam, Netherlands, pp.4-1 – 4-8.